Sequential Bone-Marrow Cell Delivery of VEGFA/S1P Improves Vascularization and Limits Adverse Cardiac Remodeling After Myocardial Infarction in Mice

Magdalena M. Żak,[1] Polyxeni Gkontra,[1] Cristina Clemente,[1] Mario Leonardo Squadrito,[2] Alessia Ferrarini,[3] Rubén A. Mota,[4] Eduardo Oliver,[5] Susana Rocha,[1] Jaume Agüero,[5,6] Jesús Vázquez,[3,6] Michele De Palma,[2] Borja Ibáñez,[5,6] and Alicia G. Arroyo[1,*,†]

[1]*Vascular Pathophysiology Area,* [3]*Proteomics Unit,* [4]*Animal Facility, and* [5]*Myocardial Pathology Area, Centro Nacional de Investigaciones Cardiovasculares (CNIC), Madrid, Spain;* [2]*École Polytechnique Federale de Lausanne (EPFL), ISREC-Swiss Institute for Experimental Cancer Research, Lausanne, Switzerland; and* [6]*CIBER-CV, Madrid, Spain.*

[†]*Present address: Centro de Investigaciones Biológicas (CIB-CSIC), Madrid, Spain.*

Microvascular dysfunction and resulting tissue hypoxia is a major contributor to the pathogenesis and evolution of cardiovascular diseases (CVD). Diverse gene and cell therapies have been proposed to preserve the microvasculature or boost angiogenesis in CVD, with moderate benefit. This study tested *in vivo* the impact of sequential delivery by bone-marrow (BM) cells of the pro-angiogenic factors vascular endothelial growth factor (VEGFA) and sphingosine-1-phosphate (S1P) in a myocardial infarction model. For that, mouse BM cells were transduced with lentiviral vectors coding for *VEGFA* or sphingosine kinase (*SPHK1)*, which catalyzes S1P production, and injected them intravenously 4 and 7 days after cardiac ischemia–reperfusion in mice. Sequential delivery by transduced BM cells of VEGFA and S1P led to increased endothelial cell numbers and shorter extravascular distances in the infarct zone, which support better oxygen diffusion 28 days post myocardial infarction, as shown by automated 3D image analysis of the microvasculature. Milder effects were observed in the remote zone, together with increased proportion of capillaries. BM cells delivering VEGFA and S1P also decreased myofibroblast abundance and restricted adverse cardiac remodeling without major impact on cardiac contractility. The results indicate that BM cells engineered to deliver VEGFA/S1P angiogenic factors sequentially may constitute a promising strategy to improve microvascularization and oxygen diffusion, thus limiting the adverse consequences of cardiac ischemia.

Keywords: VEGFA, S1P, gene–cell angiotherapy, myocardial infarction, oxygen diffusion, cardiac remodeling

INTRODUCTION

CARDIOVASCULAR DISEASE (CVD) has been the leading cause of death in the United States since the beginning of the 20th century, with almost half of those deaths caused by coronary heart disease.[1,2] The most common long-term consequence of coronary heart disease is heart failure (HF), and its prevalence increased between 2009 and 2014, in part due to the improvement in acute treatment of CVD.[2] One of the clinical manifestations of coronary heart disease is myocardial infarction (MI), which is the sudden death of myocardial tissue from ischemia caused by a blockage of a coronary artery, usually from the rupturing of an atherosclerotic plaque.[3] MI causes cardiomyocyte death, which triggers acute inflammation, angiogenesis, and finally scar formation.[4] Fibrotic scar formation is the main healing mechanism after MI due to the limited ability of the adult mammalian heart to regenerate.[3] Fibrosis causes abnormalities in both relaxation and contractility of the heart muscle, which causes ventricular remodeling, a mechanism of heart adaptation to adverse stimuli.[5] Remodeling includes left ventricular wall thinning, ventricle

*Correspondence: Dr. Alicia G. Arroyo, Vascular Pathophysiology Area, Centro Nacional de Investigaciones Cardiovasculares (CNIC), Melchor Fernández Almagro 3, 28029 Madrid, Spain. E-mail agarroyo@cnic.es

DOI: 10.1089/hum.2018.194

dilation, and changes in its shape from ellipsoid to more spherical.[6] At the cellular level, cardiomyocytes in the viable myocardium undergo hypertrophy triggered by increased load. These malformations create increasing wall stress, which causes higher myocardial oxygen demand and could cause further enlargement of the area at risk for ischemia.[7] Pathological heart remodeling caused by MI and secondary hypoxia induces HF and high mortality in the long term.[8] Indeed, HF becomes the main cause of death of patients >65 years old within 6 years after MI.[9] HF can also derive from other CVD involving microvascular dysfunction and tissue hypoxia as hypertensive cardiac hypertrophy and diabetic coronary microangiopathy.[10] For that reason, prevention and ameliorating effects of HF are of great importance.

Over the past decades, a need for an effective therapy to prevent and limit hypoxia-related cardiac adverse remodeling and as a consequence HF, particularly after MI, remains unmet. Since the introduction of fibrinolysis and angioplasty in the late 1970s, acute treatment of MI has improved dramatically, although the mortality rate caused by CVD remains high.[11] Trying to overcome the inability of adult cardiac muscle to regenerate, many therapies were implemented, including cell and gene therapies and delivery of cytokines and soluble factors. One of the aims of these therapies has been modulating angiogenesis,[12–18] since by preserving the microvasculature or boosting the formation of new vessels, tissue oxygenation would improve, alleviating adverse consequences of acute or chronic ischemia. In recent years, importance has also been given to modulating immune response after MI for its beneficial effect on heart repair.[19–22]

One of the main unsolved questions in these studies was the optimal delivery route for the factors with strategies including delivery of the recombinant protein,[23,24] gene delivery using plasmids[16,17] and modified RNA,[25] and virus-based approaches, mostly using adeno-associated virus (AAV).[14,26,27] On the other hand, cell therapies, whose main effect is believed to be based on secreting factors such as vascular endothelial growth factor A (VEGFA) and PDGF showed limited long-term improvement in cardiac vascularization.[28–30] It was hypothesized that combining two approaches by delivering cells but also transducing them to overexpress proangiogenic factors may bring an improvement in cardiac vascularization after ischemia. In the field of proangiogenic therapies, the strong proangiogenic factor VEGFA generated promising results in animal models but showed no sustained improvement in myocardial perfusion measured in the NORTHERN clinical trial.[13] However, co-delivery of VEGFA and sphingosine-1-phosphate (S1P) by AAV promoted angiogenesis and reduced cell apoptosis in a pig model of MI.[14] Of note, sequential instead of simultaneous exposure to VEGFA and S1P led to the formation of more stable vessels in scaffolds *in vitro*, but this approach has never been tested *in vivo*.[31]

This study investigated the effect of bone-marrow (BM) cells engineered to produce VEGFA or S1P and injected sequentially in improving vascularization in a preclinical mouse model of acute ischemic heart disease. Indeed, it is demonstrated that lentiviral vector (LV)-transduced BM cells injected intravenously (i.v.) in mice to deliver the pro-angiogenic factors VEGFA and S1P sequentially resulted in sustained increased vascularization 28 days after MI assessed by a newly implemented pipeline for automatized 3D image analysis of the microvasculature[32] and in contrast to the transient effect reported for non-transduced BM cells. As a consequence, the strategy also limited fibrosis and adverse cardiac remodeling. This study may offer new therapeutic possibilities for patients suffering cardiac ischemic disease.

METHODS

All experimental procedures are explained in detail in the Supplementary Methods.

LV construction and evaluation

Human *VEGFA* and *SPHK1* and *GFP* cDNAs were amplified by polymerase chain reaction and inserted downstream to the SFFV promoter of the SFFV.insert.WPRE LV backbone described in Squadrito *et al*.[33] Enzyme-linked immunosorbent assay kits were used to quantify VEGFA protein level in cell supernatants. LV transduction of BM cells was performed overnight at a multiplicity of infection of 50. The collection of cell supernatant was performed 48 and 72 h after transduction. S1P expression was measured by mass spectrometry 48 h after transduction with LV_SPHK1. For further details, see the Supplementary Methods.

Flow cytometry

BM cells were stained with antibodies against CD11b-AF647, F4/80-PE-Cy7, Ly6C-FITC, CCR2-PE, and CX_3CR1-Pacific Blue and 7-AAD live/death dye. Sample acquisition was performed using a BD LSRFortessa flow cytometer (BD Biosciences) and analyzed using FlowJo software (FlowJo LLC). Detailed staining procedure and a

list of antibodies is available in the Supplementary Methods.

Aortic ring assay

Aortic ring assay was performed, as described in Baker *et al.*[34] Mouse aortic rings were cultured in the presence of various combinations of soluble factors (rhVEGFA 30 ng/mL, S1P 1 μM) or mouse BM cells previously transduced with LVs (BM^{hVEGF}, BM^{hSPHK1}). On day 8, rings were fixed in 1.6% paraformaldehyde, and incubated overnight at 4°C with the following antibodies/reagents: IB4 or anti-CD31 (1:150) for endothelial cells and anti-smooth-muscle actin (SMA; 1:400) for mural cells. Images were acquired with a Nikon A1R confocal system coupled to a Nikon Ti-Eclipse microscope using a 10× objective and capturing 400 μm in depth with a z-stack every 3 μm. Analysis of aortic ring images was performed using Imaris software and a Matlab-based method for 3D-microvasculature developed in the lab. Reagents, antibodies, and detailed procedures are described in the Supplementary Methods.

In vivo mouse ischemia–reperfusion experiment protocol

Mice were kept at the animal facility of the Centro Nacional de Investigaciones Cardiovasculares under specific pathogen-free conditions and in accordance with the institutional guidelines. Animal procedures were approved by the corresponding legal authority of the local government of Madrid (reference number of approval PROEX/ 34/ 13). Ischemia–reperfusion (I/R) was performed in 10- to 12-week-old male BL6 mice by ligation of the left anterior descendent coronary artery for 45 min of ischemia followed by reperfusion. Echocardiography was performed 3 days after to confirm MI, and mice with a left ventricular ejection fraction (LVEF) between 20% and 40% were randomly assigned to control and treated groups. Four days post I/R, mice were injected i.v. with 5×10^6 BM^{hVEGF} in 100 μL of phosphate-buffered saline (PBS) or with PBS only as a control. Seven days post I/R, a second injection was performed with 5×10^6 BM^{hSPHK1} or PBS. On day 28, after endpoint echocardiography, hearts were weighed and collected. Echocardiography was performed using Vevo 2100 ultra high frequency ultrasound to assess cardiac parameters (end-diastolic and end-systolic volumes, stroke volume (SV), LVEF and left ventricular posterior wall thickness). Analysis of heart roundness (*i.e.*, sphericity) was performed on macroscopic images of the dissected hearts using ImageJ[35] software. Fibrosis was assessed based on Masson's trichrome staining of a series of seven levels of tissue cuts, starting from the apex to the base of the heart and visualized using NanoZoomer-2.ORS® (Hamamatsu); scar area is represented as the percentage of left-ventricular area using ImageJ software. To quantify cardiomyocyte size, an ImageJ-based semi-automated macro was designed where cardiomyocytes were recognized by laminin staining and their area and perimeter quantified. Detailed experimental procedures are described in the Supplementary Methods.

Microvasculature analysis

Sections (15 μm thick) were stained with anti-CD31, anti-PDGFRβ, and anti-SMA antibodies and with Hoechst for nuclear staining. Images were acquired with a Leica SP5 confocal microscope using a 40× objective (NA 1.25) with oil immersion with z-stacks captured every 1 μm. Analysis of the microvasculature was based on the fully automatic image analysis pipeline developed in the authors' laboratory to analyze microvascular data. The pipeline permits the calculation of a pool of parameters that quantify all major features of the vascular network. It has been described in detail in Gkontra *et al.*,[32] while a brief overview of necessary adaptations is provided in the Supplementary Methods.

Statistics

Statistical analysis was performed using GraphPad Prism v6/7. Distribution of the data sets was checked with D'Agostino–Pearson and Shapiro–Wilk normality tests, and then parametric or nonparametric tests were performed as indicated in the legends. Outliers were identified using the ROUT method ($Q = 1.000\%$).

RESULTS

Experimental design for *in vivo* sequential VEGF/S1P gene–cell angiotherapy in a MI mouse model

Sequential delivery of VEGFA (VEGF hereafter) and S1P has been shown to increase the formation of mature vessels in *in vitro* scaffolds compared to the effect of single or combined factors.[31] It was confirmed in the mouse aortic ring assay that sequential delivery of S1P after VEGF or combined delivery of the two factors induced a significantly higher proportion of sprouts, covered by SMA+ cells and a more complex vascular network than VEGF alone (Supplementary Fig. S1A and B). A decision was therefore made to test the effects of a combined gene–cell therapy in which BM cells were

boosted to produce VEGF and S1P by LV transduction and to deliver these factors sequentially. For that, LVs were generated encoding for the human *VEGF*, or *SPHK1* (sphingosine-kinase 1), the enzyme that catalyzes the conversion of the precursor sphingolipid sphingosine to the active form S1P (herein LV_ hVEGF and LV_hSPHK1, respectively). Then, the efficacy of the LV was validated in HEK and mouse BM cells transduced with LV_hVEGF and LV_hSPHK1, which indeed overexpressed VEGF and produced S1P (Supplementary Fig. S2). The proposed strategy was tested in the mouse model of acute cardiac I/R, which is closer to the human MI clinical practice. Before proceeding with the *in vivo* approach, the ability of i.v. injected BM cells to migrate to the infarcted myocardium was confirmed. Histological analysis performed 24 h after Tomato$^+$ BM cell i.v. injection confirmed the presence of red round cells in the infarct zone of hearts 4 days after I/R. Only an unspecific non-membrane-associated red signal was detected in the hearts from PBS-injected mice (Supplementary Fig. S3A).

Prior to their i.v. injection, the study also analyzed whether LV transduction and culture in the presence of stem-cell factor (SCF) and macrophage colony-stimulating factor *in vitro* impacted on the phenotype of BM cells. Following the flow cytometry gating strategy detailed in the Methods (Supplementary Fig. S3B and C), it was observed that after LV transduction with LV_hVEGF or LV_hSPHK1, the amount of neutrophils increased, macrophages decreased, and the scarce myeloid progenitors remained unchanged (Supplementary Fig. S3D–F). Notably, although no differences in the percentage of monocytes ($\sim$60%) were observed, after LV transduction, there was an increase in their CX_3CR1 cell surface expression, particularly after LV_hSPHK1 transduction with milder changes in CCR2 levels (Supplementary Fig. S3G).

BM cell-mediated delivery of VEGF and S1P improves vascularization and reduces intercapillary distances in the post-infarcted heart

Next, the study tested the *in vivo* impact of boosting BM cell sequential secretion of VEGF and S1P in a mouse model of cardiac I/R (Supplementary Fig. S4A). MI was confirmed by echocardiography 3 days post I/R, and mice with a LVEF of 20–40% were included in the study. Mice were afterwards randomly assigned to control and treated groups and then injected i.v. on day 4 post I/R with PBS or with 5×10^6 of BM^{hVEGF} followed on day 7 by PBS or 5×10^6 of BM^{hSPHK1} similar to the time points tested in the *in vitro* aortic ring assay (Supplementary Fig. S1).

Sequential VEGF/S1P angiotherapy by BM cells was primarily designed to enhance angiogenesis and increase the functional microvasculature after I/R, which may secondarily reduce post-MI adverse effects. In an effort to quantify the effect of the proposed treatment to the microvasculature in an unbiased and reproducible manner, images of transverse slices of cardiac tissue from treated and untreated subjects were analyzed by means of a 3D fully automated image analysis pipeline developed at the authors' lab.[32] The tissue was labeled for blood vessels, in particular for endothelial cells (CD31) and for SMA and PDGFRβ+ cells, and then imaged by confocal microscopy. The automated analysis approach allowed the post-MI changes of the microvasculature of the control and BM cell-delivered VEGF/S1P hearts to be compared in terms of all major microvascular characteristics: morphology, topology, angio-architecture, efficiency for oxygen diffusion, as well as its relation with SMA$^+$ and PDGFRβ^+ cells. A summary of all quantified parameters and their changes are provided in Table 1. Reference values for the parameters extracted from microvascular tissues of basal mice are also given.

Among fractal parameters, lacunarity, a parameter measuring the heterogeneity in the distribution of the size of the gaps in the tissue, significantly decreased in the infarcted area of the hearts in the treated group. This indicates a smaller dispersion of non-vascularized areas, implying a better-organized microvasculature (Table 1). Although no significant differences were observed in the overall vascular volume density 28 days after I/R, after decomposing the microvasculature into its components, that is, capillaries (CD31$^+$SMA$^-$, <5 μm), enlarged capillaries (CD31$^+$SMA$^-$, >5.1 μm), and arterioles (CD31$^+$SMA$^+$), a trend to increased capillary volume density and decreased enlarged capillaries was noticed in the infarcted zone of hearts from mice injected with BM cells delivering VEGF/S1P compared to controls (Fig. 1A–C and Table 1). There were, however, no changes in the volume density and the percentage of arterioles (Fig. 1B and C). Accordingly, treatment also resulted in significantly more abundant endothelial cells in the vasculature of the infarcted zone (Fig. 1A). Interestingly, in the remote zone, a significant increase in the volume and percentage of capillaries and a decrease in the percentage of enlarged capillaries were also observe in hearts from the VEGF/S1P-treated group, in spite of the lack of statistically significant between-group differences

Table 1. *Quantitative analysis of microvasculature parameters in the cardiac tissue from treated and non-treated mice after myocardial infarction*

	Infarct untreated	*Infarct treated*	*Remote untreated*	*Remote treated*	*Basal*
Fractal-based metrics					
Fractal dimension	1.79 ± 0.04	1.78 ± 0.03 ↓	1.86 ± 0.04	1.85 ± 0.04 ↓	1.91 ± 0.01
Lacunarity ($\times 10^{-2}$)	96.42 ± 0.84	95.84 ± 1.16 ↓	92.34 ± 0.94	91.46 ± 0.83 ↓*	90.93 ± 0.15
Minkowski-based metrics					
Vascular volume density (%)	2.62 ± 0.38	2.46 ± 0.26 ↓	3.66 ± 1	3.44 ± 0.8 ↓	3.48 ± 0.21
Vascular surface area density ($\times 10^{-3}$; $\mu m^2/\mu m^3$)	23.79 ± 1.51	24.86 ± 3.13 ↑	41.72 ± 6.31	43.08 ± 5.15 ↑	40.17 ± 1.91
Breadth density ($\times 10^{-3}$; $\mu m/\mu m^3$)	0.97 ± 0.06	1.08 ± 0.23 ↑	2.23 ± 0.31	2.38 ± 0.22 ↑	2.05 ± 0.22
Euler characteristic density ($\times 10^{-5}$; $1/\mu m^3$)	−1.7 ± 3.09	−1.2 ± 2.87 ↑	1.6 ± 6.89	3.49 ± 9.56 ↑	5.89 ± 1.76
Capillary volume density (%)	0.66 ± 0.15	0.76 ± 0.17 ↑	2.31 ± 0.39	2.65 ± 0.31 ↑*	2.36 ± 0.13
Capillary surface area density ($\times 10^{-3}$; $\mu m^2/\mu m^3$)	9.94 ± 2.5	11.24 ± 2.75 ↑	32.49 ± 4.57	37.1 ± 2.69 ↑**	32.47 ± 2.08
Enlarged capillary volume density (%)	0.58 ± 0.34	0.34 ± 0.21 ↓	0.81 ± 0.63	0.4 ± 0.43 ↓	0.3 ± 0.16
Enlarged capillary surface area density ($\times 10^{-3}$; $\mu m^2/\mu m^3$)	4.84 ± 2.55	2.93 ± 1.7 ↓	6.69 ± 5.11	3.47 ± 3.68 ↓	2.51 ± 1.45
SMA+ vessel volume density (%)	1.37 ± 0.24	1.35 ± 0.16 ↓	0.53 ± 0.27	0.39 ± 0.26 ↓	0.82 ± 0.1
SMA+ vessel surface area density ($\times 10^{-3}$; $\mu m^2/\mu m^3$)	10.21 ± 1.73	11.67 ± 1.67 ↑	4.12 ± 1.78	3.55 ± 2.6 ↓	6.18 ± 0.33
Capillary (%)	26.42 ± 9.74	31.11 ± 7.53 ↑	66.19 ± 15.86	78.94 ± 10.78 ↑*	67.92 ± 3.57
Enlarged capillary (%)	21.05 ± 10.45	13.6 ± 6.98 ↓	19.95 ± 13.19	9.95 ± 8.48 ↓*	8.53 ± 4.54
SMA+ vessel (%)	52.52 ± 6.81	55.29 ± 5.89 ↑	13.86 ± 4.84	11.11 ± 6.6 ↓	23.55 ± 2.56
Graph-based metrics					
Vascular segment diameter (μm)	4.23 ± 0.7	3.96 ± 0.6 ↓	3.76 ± 0.62	3.43 ± 0.37 ↓	3.91 ± 0.25
Vascular segment length (μm)	8.58 ± 1.55	8.58 ± 1.4 ↓	9.67 ± 1.23	10.06 ± 1.06 ↑	12.24 ± 1.62
Vascular segment surface (μm^2)	119.08 ± 38.82	112.19 ± 30.08 ↓	121.14 ± 31.15	114.62 ± 18.95 ↓	153.61 ± 26.72
Vascular segment volume (μm^3)	149.58 ± 67.97	132.71 ± 48.83 ↓	135.32 ± 52.18	113.56 ± 27.61 ↓	175.04 ± 37.32
Tortuosity ($\mu m/\mu m$)	1.5 ± 0.06	1.54 ± 0.06 ↑	1.51 ± 0.08	1.54 ± 0.06 ↑	1.47 ± 0.01
SMA+ and Pdgfrb-related metrics					
Myofibroblasts abundance	0.5 ± 0.06	0.43 ± 0.09 ↓*	0.04 ± 0.03	0.03 ± 0.02 ↓	0.02 ± 0.01
Vessels covered with Pdgfrb (%)	76.95 ± 8.09	76.59 ± 11.75 ↓	87.07 ± 7.1	87.21 ± 5.71 ↑	88.75 ± 2.85
Vessels covered with SMA (%)	38.19 ± 4.82	40.98 ± 5.7 ↑	15.98 ± 6.07	12.26 ± 6.01 ↓	24.18 ± 3.27
SMA+ layer thickness (μm)	3.72 ± 0.82	3.68 ± 0.51 ↓	3.85 ± 0.39	3.7 ± 0.79 ↓	4.5 ± 0.52
SMA+ perivascular cells[a]	16.19 ± 3.65	18.33 ± 4.39 ↑	6.1 ± 2.78	4.93 ± 2.56 ↓	8.33 ± 0.66
Efficiency in oxygen diffusion					
Median extravascular distance (μm)	13.38 ± 1.52	11.76 ± 2.21 ↓	5.68 ± 0.51	5.34 ± 0.28 ↓	5.63 ± 0.35
Maximal extravascular distance (μm)	43.63 ± 7.04	36.02 ± 8.59 ↓*	12.53 ± 1.2	11.69 ± 0.76 ↓	13.19 ± 1
Additional cell-related metrics					
Endothelial cells ($\times 10^5$)[b]	26.71 ± 2.37	30.31 ± 4.28 ↑*	35.43 ± 5.83	39.79 ± 6.04 ↑	31.63 ± 4.75

The mean ± standard deviation of all parameters for cardiac tissue from treated (BM^{hVEGF} + BM^{hSPHK1}) and non-treated (phosphate-buffered saline) mice along with pairwise comparisons among the different tissue conditions. Capillaries correspond to CD31+ and SMA– vessels of diameter <5 μm, enlarged capillaries to CD31+ and SMA– vessels of diameter ≥5 μm, and SMA+ vessels to CD31+ and SMA+ vessels regardless their diameter. Up and down arrows indicate increase and decrease, respectively, of the parameter value for (1) tissue from infarcted areas of subjects treated with BM^{hVEGF} + BM^{hSPHK1} compared to tissue from infarcted areas of untreated subjects, and (2) tissue from remote areas of subjects treated with BM^{hVEGF} + BM^{hSPHK1} compared to tissue from remote areas of untreated subjects.

[a]Number per mm vascular length.

[b]Number per mm^3 vascular volume.

*$p < 0.05$; **$p < 0.01$. The p-values were calculated by means of a two-sample t-test.

BM, bone marrow; VEGF, vascular endothelial growth factor; SPHK1, sphingosine kinase; SMA, smooth-muscle actin.

in overall vascular volume density. Concomitantly, endothelial cell abundance in the remote zone was slightly increased in the treated group (Fig. 1D–F). These findings indicate that combined delivery of VEGF/S1P impacted mostly on the capillaries, increasing their volume density and the endothelial cell content while decreasing their remodeling/enlargement in both the infarcted and the remote zones.

The main function of the microvasculature is to provide nutrients and oxygen to the heart, particularly after ischemia, to preserve cell viability and promote repair. Thus, toward obtaining insights into the efficiency of the network for oxygen diffusion, traditional indicators of oxygen diffusion (*i.e.*, maximal extravascular distances) were studied by means of the automated pipeline. According to the larger proportion of capillaries and higher endothelial cell numbers, maximal extravascular distances were significantly reduced in the infarct zone of hearts from mice injected with BM cells producing VEGF and S1P 28 days after I/R compared to the controls, indicating better oxygen diffusion. A similar trend to reduced extravascular distances was observed in the remote zone of treated mice (Fig. 2).

Next, the study sought to decipher the contribution of VEGF and S1P overexpression versus

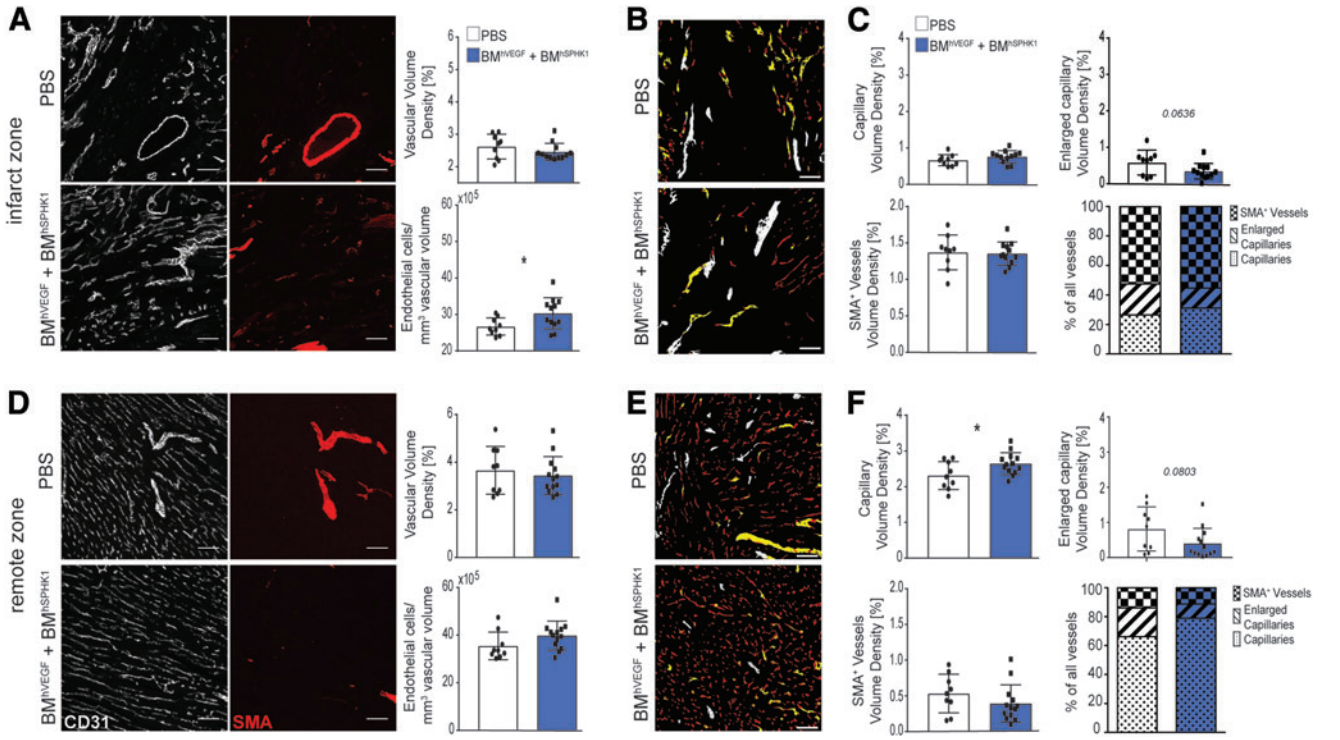

Figure 1. Sequential bone marrow (BM) cell delivery of vascular endothelial growth factor (VEGF) and sphingosine-1-phosphate (S1P) increases capillary volume density and endothelial cell number on the infarcted heart post myocardial infarction (MI). **(A)** *Left panels*: representative maximal intensity projections from confocal microscopy images of transverse sections of mouse hearts stained for endothelial cells (CD31, *gray*) and smooth-muscle cells (SMA, *red*). *Right panels*: bar graphs showing total vascular volume density and the number of endothelial cells per vascular volume in the infarct zone of treated and non-treated mice 28 days post ischemia–reperfusion (I/R). Scale bar: 50 μm. **(B)** Representative images of segmented vessels in three categories: capillaries ($CD31^+SMA^-$, <5 μm diameter, *red*), enlarged capillaries ($CD31^+SMA^-$, >5.1 μm diameter, *yellow*), and arterioles/SMA+ vessels ($CD31^+SMA^+$, *white*) in the infarct zone of treated and non-treated hearts. Scale bar: 50 μm. **(C)** Bar graphs showing volume densities for the three-vessel categories, as well as percentage representation of each vessel type out of the total vasculature. **(D–F)** Representative images and bar graphs, as described in **(A–C)**, corresponding to the remote zone of hearts from treated and non-treated mice 28 post I/R. Data represent the mean ± *SD* of 9 and 12 mice for non-treated and treated groups, respectively, analyzed in two independent experiments. A parametric *t*-test was used for statistical comparison. *$p<0.05$; **$p<0.01$; ***$p<0.001$. Color images are available online.

endogenous secretion of factors by BM cells to the myocardial angiogenic phenotype, since PBS was used as *in vivo* control. Non-transduced BM cells did not increase vascular sprouting versus control medium in the aortic ring in contrast to sequential exposure to BM cells secreting VEGF and S1P, which induced a significant increase in vascular sprouts with a good proportion covered by SMA+ cells, indicative of stable vessels, and a more complex vascular network (Supplementary Fig. S4B). These findings argue in favor of overexpressed VEGF and S1P by LV-transduced BM cells as the factors responsible for boosting capillarization post MI.

Sequential BM cell delivery of VEGF and S1P diminishes post-infarction tissue fibrosis with no impact on cardiac contractility

After MI, dead cardiomyocytes are mostly replaced by fibrotic tissue, reducing cardiac pump function. The study analyzed whether improved capillarization and oxygen diffusion by BM cell sequential delivery of VEGF/S1P had any impact on cardiomyocyte survival and thus in cardiac performance. Despite the presence of isolated clusters of viable cardiomyocytes within the scar of infarcted hearts from VEGF/S1P-treated mice but not in untreated controls 28 days post-I/R (Supplementary Fig. S5A), echocardiography analysis showed no significant between-group differences in the reduced LVEF and the SV (Supplementary Fig. S5B and C).

Regardless the ejection fraction values, fibrosis extent and tissue stiffness are the major factors driving post-MI progression to HF. Therefore, although a major impact of the BM cell-VEGF/S1P therapy could not be observed on cardiac contractility, next fibrosis-related parameters were assessed, since cardiac injury and hypoxia are enhancers of the myofibroblast-driven fibrotic program.[36,37] Between-group differences could not be detected in the total scar volume of the left ventricular free wall calculated from serial Masson-stained sections

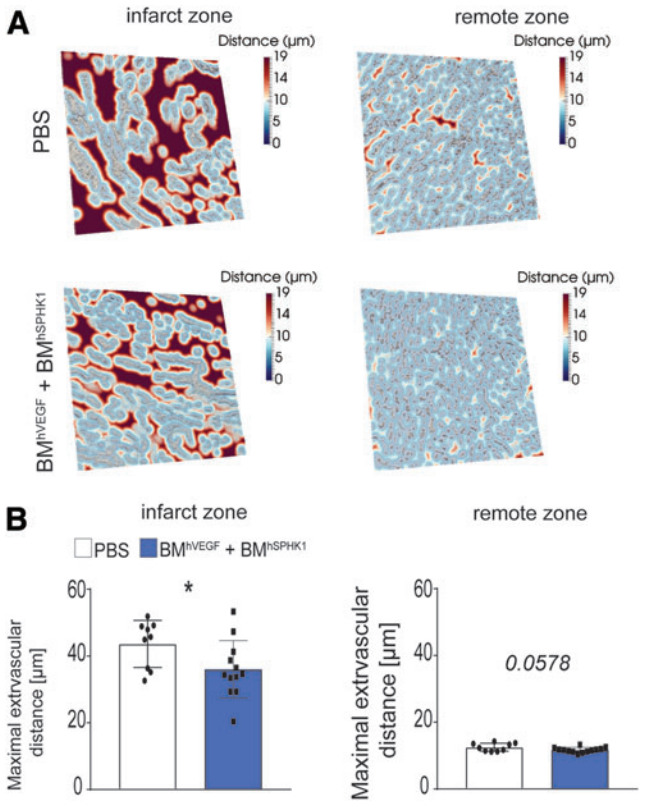

Figure 2. BM cell sequential delivery of VEGF and S1P reduces intercapillary distances in the post-infarcted heart. **(A)** Representative images of extravascular distance maps from the infarct and remote zone of treated and control mice 28 days post MI. **(B)** Bar graphs show the quantification of maximal extravascular distances in the conditions shown in **(A)**. Data are represented as the mean ± standard deviation (*SD*) of 9 and 12 mice for non-treated and treated groups, respectively, analyzed in two independent experiments. A parametric *t*-test was used for statistical comparison. $*p<0.05$; $**p<0.01$; $***p<0.001$. Color images are available online.

spanning the whole heart 28 days post I/R (Fig. 3A and B). However, the cardiac section closest to the valves consistently showed a significantly reduced scar area in the BM cell VEFG/S1P-treated group (Fig. 3C). Complementarily, using the images of mouse cardiac tissues stained for PDGFRβ and CD31, the myofibroblast abundance were also automatically quantitated as the ratio of the volume of myofibroblasts over the volume of all PDGFRβ+ cells. In this approach, myofibroblasts are considered PDGFRβ+ areas that are not in touch with the vessels.[32,38] Following this approach, significantly reduced myofibroblast abundance was noticed in the infarct zone of hearts from BM cell VEGF/S1P-treated mice compared to untreated controls. Myofibroblasts were barely detected, but there were fewer in the remote zone of the treated group (Fig. 3D and E and Table 1). Since myofibroblasts are in charge of secreting and remodeling extracellular matrix proteins, particularly collagens, to form the scar, myofibroblast reduction prompted collagen fiber organization and condensation to be analyzed, in spite of no significant differences observed in overall scar area. Analysis of first-order features of collagen fibrils in second harmonic generation microscopy images revealed increased skewness and kurtosis in the collagen fibers of the scar from infarcted hearts of the BM cell VEGF/S1P-treated group compared to controls (Fig. 3F and G). These values would indicate thinner and underdeveloped collagen fibers and thus lower tissue stiffness.[39]

VEGF and S1P sequential delivery by BM cells limits adverse cardiac remodeling post MI

One of the consequences of MI is cardiac remodeling defined as the post-damage alterations that result in acute and chronic changes of heart size, mass, geometry, and function, which may finally lead to cardiac dysfunction and HF.[40] First, ventricle cavity size and wall thickness were quantitated, and a trend was observed of reduced dilatation and thickening of the left ventricle in the VEGF/S1P-treated mice 28 days post I/R (Fig. 4A and B). Since volume and thickness changes are not fully developed 4 weeks after I/R in mice,[41] global cardiac geometry was also analyzed, which is modified more acutely.[40] It was found that hearts from BM cell VEGF/S1P-treated mice kept their ellipsoid-like shape in contrast to those from untreated control mice that became significantly rounder at 28 days post I/R, as expected (Fig. 4C). Moreover, analysis of cardiomyocytes in the remote zone, which usually become hypertrophic in response to post-MI left ventricular stiffness and volume overload,[40] showed that cardiomyocytes in the remote zone of hearts from BM cell VEGF/S1P-treated mice became less hypertrophic, with significantly smaller area and perimeter compared to control mice 28 days post I/R (Fig. 4D and E). Finally, cardiac remodeling also results in changes at the molecular level, with proteins increasing (collagen type I) or decreasing (Atpa2a/Serca2a) during the process.[40] Notably, VEGF/S1P treatment led to decreased collagen type I and increased Atp2a2 (Serca2) protein levels in heart extracts compared to untreated mice 28 days post I/R (Fig. 4F and G), confirming that the angiotherapy ameliorated adverse cardiac remodeling.[40]

Collectively, these findings indicate that sequential VEGF/S1P gene–BM cell therapy limits post-MI adverse cardiac remodeling consistent with the enhanced capillarization and oxygen diffusion effects and reduced myofibroblast abundance in the infarcted tissue.

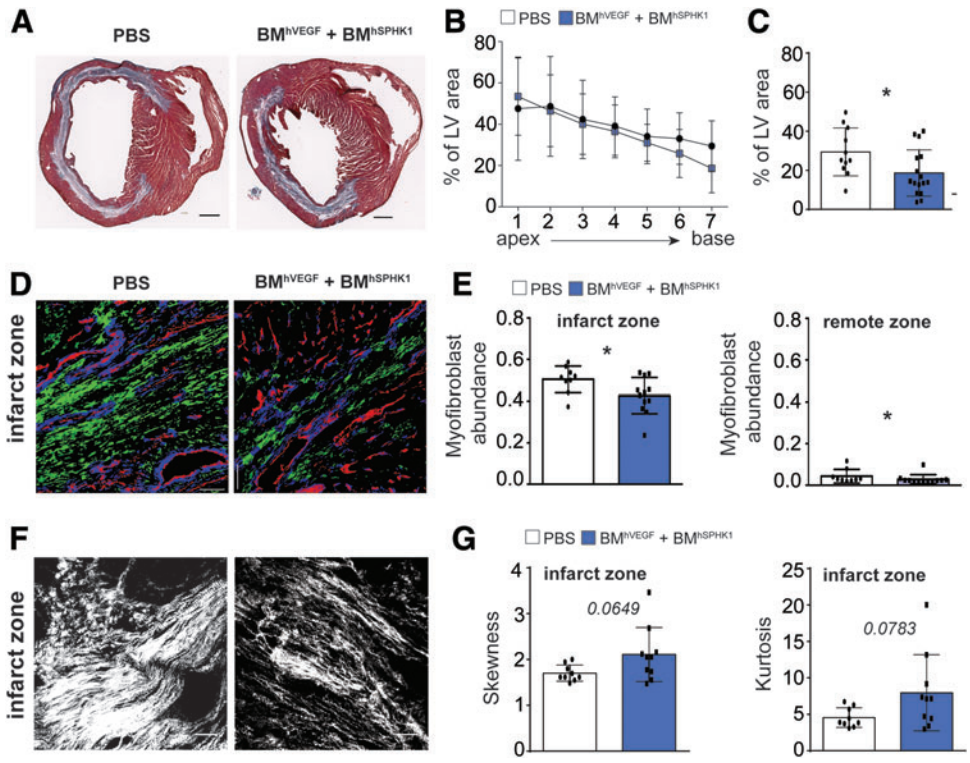

Figure 3. Sequential BM cell-secreted VEGF and S1P angiotherapy reduces myofibroblast abundance and collagen fiber compaction in the infarcted heart post I/R. **(A)** Representative images from Masson's trichrome-stained transverse sections of hearts from treated and control groups 28 days post I/R. **(B)** Graphs shows the percentage of the left ventricular area covered by scar tissue in serial cuts spanning the whole heart from the apex (1) to the base (7). **(C)** Bar graph shows the percentage of left ventricular scar area in the transverse section of the base of the heart (closest to the valves). **(D)** Pseudo-colored representation of confocal microscopy images of transverse sections from the infarct zone of treated and control hearts stained for CD31 and PDGFRβ in which vessels (CD31$^+$) are shown in *red*, perivascular cells (PDGFRβ^+ cells touching vessels) in *blue*, and myofibroblasts (PDGFRβ^+ cells distant from the vessels) in *green*. **(E)** Bar graphs represent myofibroblast abundance in the infarct and remote zones. **(F)** Representative images of collagen fibers obtained by second harmonic generation (SHG) multiphoton microscopy in transverse sections of hearts from treated and control groups 28 days post I/R. **(G)** Bar graphs show the quantitation of the first-order parameter skewness (asymmetry of pixel distribution) and kurtosis (gray-tone spread-out distribution) in SHG images. Data are represented as the mean $\pm$ *SD*. $n=11$ and 16 **(B** and **C)**, $n=9$ and 12 **(D** and **E)**, and $n=9$ and 10 **(F** and **G)** mice of non-treated and treated groups, respectively, analyzed in three **(B** and **C)** and two **(D–G)** independent experiments. Data were statistically compared by **(B)** two-way analysis of variance (ANOVA), **(C)** parametric *t*-test, and **(D–G)** nonparametric Mann–Whitney *U*-test. $*p<0.05$; $**p<0.01$; $***p<0.001$. Color images are available online.

DISCUSSION

This study tested the effect of sequential delivery by BM cells of the proangiogenic factors VEGF and S1P on boosting angiogenesis and/or preserving the microvasculature after MI *in vivo*. The intervention succeeded in increasing endothelial cell numbers and capillaries and diminishing adverse angioadaptation, thus improving oxygen diffusion 4 weeks after the ischemic event. In spite of no major effect on cardiac contractility, BM cell

Figure 4. Sequential delivery of VEGF and S1P by lentiviral vector (LV)-transduced BM cells limits adverse cardiac remodeling post MI. **(A)** Graphs show the left ventricular end-systolic (LVESV) and end-diastolic (LVEDV) volumes of hearts from basal (no I/R) and from control (PBS) or VEGF/S1P-treated mice at 3 and 28 days post I/R. **(B)** Graph shows the left ventricular posterior wall end-diastolic thickness calculated in M-mode ultrasound images in hearts from control (PBS) or VEGF/S1P-treated mice at 28 days post I/R. **(C)** Bar graphs show the heart roundness coefficient quantitated in macroscopic images from hearts of treated and non-treated mice 28 days post I/R. **(D)** Maximal intensity projections from confocal microscopy images of the remote area from pan-laminin (green)-stained transverse sections of hearts from treated and non-treated mice 28 days post I/R. Scale bar: 50 μm. **(E)** Bar graphs show the quantification of cardiomyocyte area and perimeter from pan-laminin-stained images **(D)**. **(F)** Representative Western blots for Col1a1 and Atp2a2 protein expression in hearts from treated and non-treated mice 28 days post I/R (*top*) and graphs with the quantification expressed as fold change (F.C., *bottom*). Tubulin is included as loading control. $n=6$ mice from non-treated (PBS) and treated (BM^{hVEGF}+BM^{hSPHK1}) groups. Data are shown as the mean $\pm$ standard error of the mean and were statistically compared with a parametric *t*-test ($*p<0.05$). **(G)** Representative maximal intensity projections from confocal microscopy images of heart sections from treated and non-treated mice 28 days post I/R stained for cardiomyocytes (α-actinin, *gray*) and Atp1a2 (*red*). *Yellow squares* indicate the magnified areas. Scale bar: 100 and 50 μm in the magnified views. Data represent the mean $\pm$ *SD*. $n=6$ mice for non-I/R and $n=11$–12 and 16–18 mice for non-treated and treated groups, respectively, analyzed in three independent experiments **(A–E)**. $n=6$ mice for non-treated and treated groups, respectively, analyzed in two independent experiments **(F)**. Data were statistically compared with one-way ANOVA **(A)** and a parametric *t*-test **(B–F)**. $*p<0.05$; $**p<0.01$; $***p<0.001$. Color images are available online.

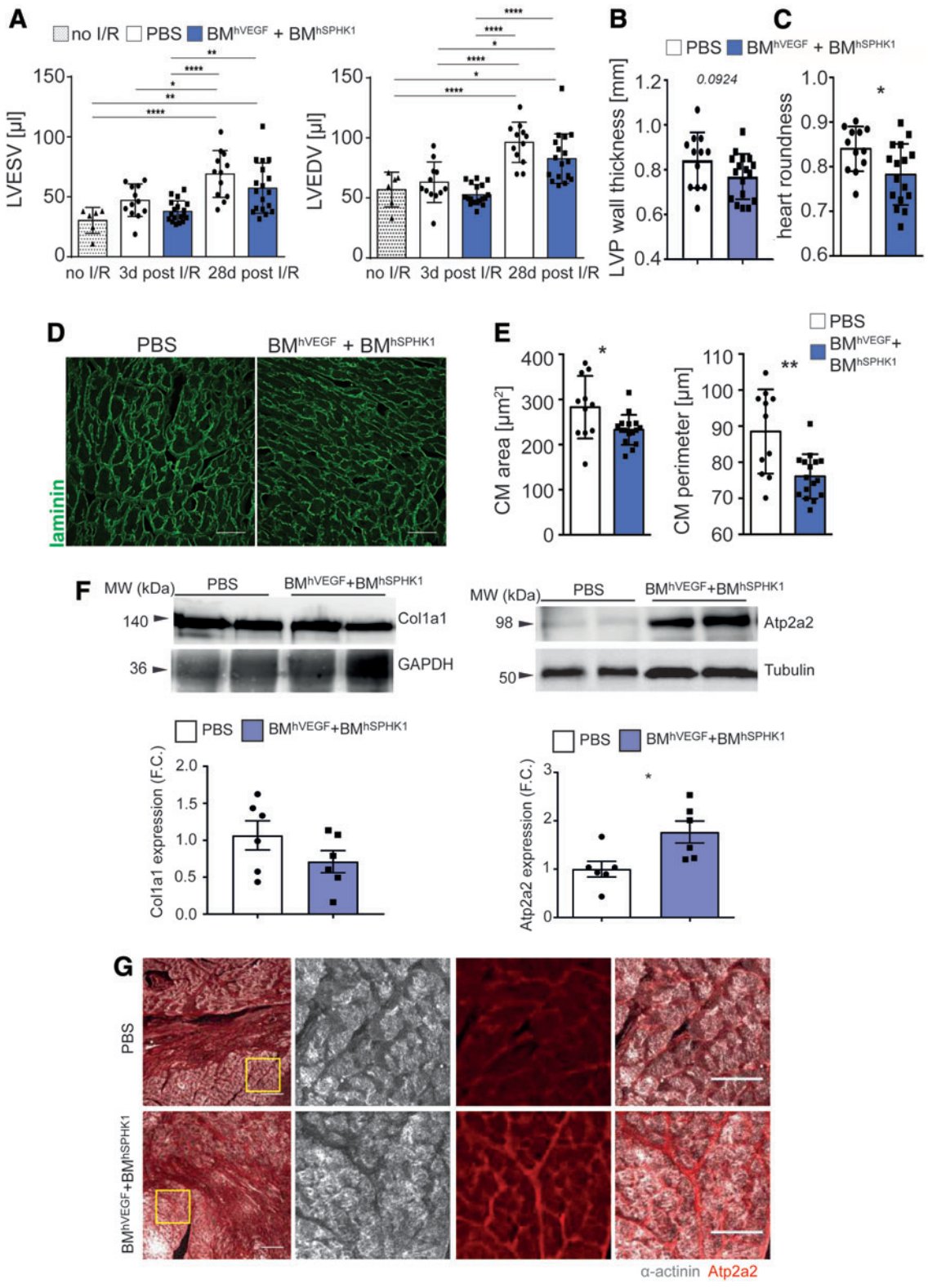

sequential VEGF/S1P therapy also reduced myofibroblast-driven tissue fibrosis and limited adverse post-MI cardiac remodeling.

In terms of safety and possible translation of this therapy, LV transduction is performed *ex vivo*, and the injected cells are mostly differentiated. This would limit the possibility of transferring the LV to other cell types in the organism and reduce risks of genetic alterations in the hematopoietic progenitors and their progeny by LV insertion. Previous analysis in the pig infarcted heart showed that on day 3 post MI, the 3D structure of the microvasculature is mostly preserved, but its function starts to decline, as manifested by the larger extravascular distances causing disturbed oxygen diffusion.[32] Endogenous angiogenesis after MI occurs during the first 2 weeks after the ischemic event. Thus, detailed kinetics of the endothelial cell marker PECAM1/CD31 in a mouse model of permanent coronary artery ligation showed an increase in endothelial cells at 2 days with a maximum at 4 days and then a decline and return to baseline levels 7 days after MI.[4,36,42,43] These findings support the vascular boosting intervention 4 days post MI.

This study analyzed the impact of the BM cell VEGF/S1P therapy at the 28-day endpoint post I/R. Notably, persistent benefits were observed from this strategy in contrast to previously reported therapeutic approaches in which effects on the vasculature were often transient. For example, the intramyocardial injection of mesenchymal stem cells showed benefits in perfusion on the infarcted area at the first week but not after 4 weeks.[44] This newly implemented BM cell VEGF/S1P therapy mainly induced an increase in the abundance of endothelial cells and reduced extravascular distances in the infarcted area of hearts from treated mice. Concomitantly, trends toward decreased presence of enlarged capillaries were observed. These effects might indicate reduced angioadaptation, which normally occurs in response to capillary loss and flow redistribution in the remaining vessels.[32,45] Previous proangiogenic therapies, including AAV-mediated overexpression of VEGF and ANG1 in a pig model of MI,[14] plasmid-mediated overexpression of bFGF and PDGF in a rat model of MI,[46] and microcapsule release of FGF2 and HGF in a rat model of HF,[47] improved the cardiac vasculature by increasing both capillary and arteriole/large-vessel content. As it is becoming recently accepted, interventions in the cardiac stroma[48] as the microvasculature may secondarily lead to reduced CM death, tissue damage, and fibrosis, since this is often triggered by tissue hypoxia.[37]

The intervention was based on previous reports showing that sequential VEGF and S1P actions were of benefit to induce stable vessels in scaffolds *in vitro*.[31] VEGF is a proangiogenic factor, which induces endothelial cell migration, proliferation, and survival, depending on the endothelial cell context, and at high persistent levels may induce vascular leakiness and regression.[49,50] The increase in endothelial cell number in the infarcted area of hearts from treated mice suggests an overall effect of VEGF in endothelial cell proliferation and/or survival. Moreover, stimulation of endothelial cells with VEGF causes overexpression of S1P1 receptors on these cells and, in isolated arteries, enhances S1P-mediated vasorelaxation and eNOS phosphorylation.[31] This effect may contribute further to pro-survival and proangiogenic programs in the capillary endothelium. It is worth mentioning that although VEGF and S1P are endogenously produced in the heart, cell-type transcriptomics analysis in the pig heart revealed decreased mRNA levels of *VEGF* and *SPHK1* 3 days post I/R (unpublished data), supporting the rationale of boosting VEGF/S1P tissue levels by LV-BM delivery. S1P itself is considered a master regulator of signaling pathways involved in cardiac improvement after MI, and it has lately attracted attention as a possible target.[51] It cannot be ruled out that S1P secreted locally by the transduced BM cells in the infarcted area could have, in addition to enhanced capillarization, some direct impact on cardiomyocyte survival and thus on reducing cardiac damage. Nonetheless, the lack of major differences in the infarct size argues against a major role of this protection mechanism. Furthermore, in contrast to the reported S1P effect on myofibroblasts,[51] reduced myofibroblast abundance is observed, suggesting that S1P paracrine effects on cell types other than endothelial cells seem unlikely. Autocrine effects, however, may still be possible, since transduction with LV_hVEGF or LV_hSPHK1 resulted in BM-derived monocytes with higher CX_3CR1 levels, which may enhance their early traffic to the damaged heart.[52] In this line, higher expression of the CX_3CR1 receptor on circulating $Ly6C^{low}$ monocytes has been shown to induce a positive effect on their recruitment and the promotion of angiogenesis in the injury site in hind-limb ischemia[53] and carotid injury[54] models. Moreover, S1P can promote an anti-inflammatory phenotype in macrophages through activation of their S1P1 receptor after damage and contribute to macrophage-mediated cardiac repair.[55] This pos-

sibility merits further analysis with macrophage specific markers. Of note, significantly increased capillaries and a trend to diminished extravascular distances were also observed in the remote zone of BM cell VEGF/S1P-treated infarcted mice, suggesting that LV-BM cells can also induce vascular effects in that area.[56]

VEGF/S1P gene–cell therapy did not improve post-MI cardiac contractility in accordance with other previously reported strategies. Nevertheless, in spite of no major impact on contractility, VEGF/S1P combined angiotherapy limited post-MI adverse cardiac remodeling, as demonstrated by the preserved cardiac geometry and cardiomyocyte morphology in the remote zone, as well as the higher Atp2a2 protein levels. The reduced cardiac sphericity induced by the angiotherapy supports its clinical relevance, since it has been related to post-MI long-term survival.[57] This improvement may be related to the reduced collagen stiffness and myofibroblast abundance in the infarcted area but also in the remote zone of hearts from the treated mice.[58] Whether remote changes are directly related to the therapy or indirectly as a consequence of the effects on the scar properties (better perfusion, lower stiffness) in the infarcted area remains to be elucidated. Moreover, since cardiac macrophages proliferate in response to mechanical stretching caused by stiffer failing myocardium,[20] the reduced collagen stiffness in treated mice may also explain the trend to lower amount of macrophages in the remote zone observed in these mice (unpublished data).

There were fewer functional beneficial effects of the angiotherapy than expected, despite a consistent biological effect on histology endpoints. This may be related to insufficient factor concentration in the *in vivo* experiments, and more dramatic effect needs to be induced to elicit relevant functional changes. In this regard, future studies with higher transgene overexpression, or more effective gene–cell delivery systems (intracoronary, trans-endocardial) may overcome the limitations observed in the murine model.[59]

This work presents some limitations, which require future studies. First, in this study, gene–cell therapy was compared to a placebo to acquire a clear determination of its efficacy. Although the absence of angiogenic effects induced by non-transduced BM cells on the mouse aortic rings argue in favor of specific effects of sequential delivery of VEGF plus S1P on the phenotype observed in the microvasculature 28 days post MI, comparison with injection of wild-type or LV mock-transduced BM cells would help establish the precise contribution of paracrine signaling by the BM cells versus the delivered VEGF/S1P *in vivo*. Second, deciphering the actual impact of the combined gene–cell VEGF and S1P therapy on the microvasculature, cardiomyocyte survival, and/or monocyte/macrophage subsets will require deeper analysis at earlier time points after ischemia. Third, the benefits of this strategy have only been tested in the I/R model by its proximity to clinical practice. It will also be of interest to evaluate the impact of combined VEGF/S1P gene–cell therapy in the extensively used permanent left anterior descending coronary artery ligation in which arterialization is relevant for revascularization, as well as in CVD involving chronic cardiac ischemia. Forth, in terms of global cardiac function, clinical trials using intracoronary injection of whole BM showed no long-term improvement in LVEF after MI,[60,61] despite promising short-term effects.[62,63] Therefore, analysis of the impact of BM cell VEGF/S1P therapy at longer time points after cardiac ischemia is guaranteed to elucidate whether the beneficial effects on cardiac remodeling persist in time.

In sum, this study offers a novel therapeutic strategy based on sequential BM cell delivery of angiogenic factors to enhance micro-vascularization and oxygen diffusion, thus limiting the adverse consequences of cardiac ischemic diseases.

ACKNOWLEDGMENTS

We thank Mónica Gómez for her help with I/R surgery, Lorena Flores and Ana Vanessa Alonso López for performing and analyzing echocardiography, Dr. Manuel Lobo for ultrasound image analysis, Drs. Borreguero and Maria Villalba for their help in interpreting the results, and Verónica Labrador and CNIC's Microcopy Unit for their expertise and help with image analysis.

This study was supported by grants from the Spanish Ministerio de Ciencia, Innovación y Universidades SAF2014-52050-R and SAF2017-83229-R to A.G.A. and BIO2015-67580-P to J.V. and the Carlos III Institute of Health-Fondo de Investigación Sanitaria (PRB2, IPT13/0001-ISCIII-SGEFI/FEDER, ProteoRed). The research leading to these results received funding from the People Programme (Marie Curie Action) of the European Union's Seventh Framework Programme (FP7/2007-2013) under REA grant Agreement 608027. The CNIC is supported by the Spanish Ministerio de Ciencia, Innovación y Universidades and the Pro-CNIC Foundation, and is a Severo Ochoa Center of Excellence (award SEV-2015-0505).

AUTHOR DISCLOSURE

No competing financial interests exist.

SUPPLEMENTARY MATERIAL

Supplementary Methods

Supplementary Fig. S1
Supplementary Fig. S2
Supplementary Fig. S3
Supplementary Fig. S4
Supplementary Fig. S5

REFERENCES

1. Mendis S, Puska P, Norrving B, et al. Global Atlas on Cardiovascular Disease Prevention and Control. Geneva, Switzerland: World Health Organization in collaboration with the World Heart Federation and the World Stroke Organization, 2011.
2. Benjamin EJ, Blaha MJ, Chiuve SE, et al. Heart disease and stroke statistics—2017 update: a report from the American Heart Association. Circulation 2017;135:e146–e603.
3. Frangogiannis NG. Pathophysiology of myocardial infarction. Compr Physiol 2015;5:1841–1875.
4. Matsui Y, Morimoto J, Uede T. Role of matricellular proteins in cardiac tissue remodeling after myocardial infarction. World J Biol Chem 2010;1:69–80.
5. Schirone L, Forte M, Palmerio S, et al. A review of the molecular mechanisms underlying the development and progression of cardiac remodeling. Oxid Med Cell Longev 2017;2017:3920195.
6. Jessup M, Brozena S. Heart failure. N Engl J Med 2003;348:2007–2018.
7. Bhatt AS, Ambrosy AP, Velazquez EJ. Adverse remodeling and reverse remodeling after myocardial infarction. Curr Cardiol Rep 2017;19:71.
8. Taimeh Z, Loughran J, Birks EJ, et al. Vascular endothelial growth factor in heart failure. Nat Rev Cardiol 2013;10:519–530.
9. Torabi A, Cleland JG, Rigby AS, et al. Development and course of heart failure after a myocardial infarction in younger and older people. J Geriatr Cardiol 2014;11:1–12.
10. Pieske B, Wachter R. Impact of diabetes and hypertension on the heart. Curr Opin Cardiol 2008; 23:340–349.
11. Bennett J, Dubois C. Percutaneous coronary intervention, a historical perspective looking to the future. J Thorac Dis 2013;5:367–370.
12. Doppler SA, Deutsch MA, Lange R, et al. Cardiac regeneration: current therapies—future concepts. J Thorac Dis 2013;5:683–697.
13. Stewart DJ, Kutryk MJ, Fitchett D, et al. VEGF gene therapy fails to improve perfusion of ischemic myocardium in patients with advanced coronary disease: results of the NORTHERN trial. Mol Ther 2009;17:1109–1115.
14. Tao Z, Chen B, Tan X, et al. Coexpression of VEGF and angiopoietin-1 promotes angiogenesis and cardiomyocyte proliferation reduces apoptosis in porcine myocardial infarction (MI) heart. Proc Natl Acad Sci U S A 2011;108:2064–2069.
15. Hedman M, Hartikainen J, Syvanne M, et al. Safety and feasibility of catheter-based local intracoronary vascular endothelial growth factor gene transfer in the prevention of postangioplasty and in-stent restenosis and in the treatment of chronic myocardial ischemia: Phase II results of the Kuopio Angiogenesis Trial (KAT). Circulation 2003;107:2677–2683.
16. Kastrup J, Jorgensen E, Ruck A, et al. Direct intramyocardial plasmid vascular endothelial growth factor-A165 gene therapy in patients with stable severe angina pectoris A randomized double-blind placebo-controlled study: the Euroinject One trial. J Am Coll Cardiol 2005;45:982–988.
17. Vera Janavel GL, De Lorenzi A, Cortes C, et al. Effect of vascular endothelial growth factor gene transfer on infarct size, left ventricular function and myocardial perfusion in sheep after 2 months of coronary artery occlusion. J Gene Med 2012;14: 279–287.
18. Ieda M, Fu JD, Delgado-Olguin P, et al. Direct reprogramming of fibroblasts into functional cardiomyocytes by defined factors. Cell 2010;142: 375–386.
19. Nahrendorf M, Swirski FK, Aikawa E, et al. The healing myocardium sequentially mobilizes two monocyte subsets with divergent and complementary functions. J Exp Med 2007;204:3037–3047.
20. Sager HB, Hulsmans M, Lavine KJ, et al. Proliferation and recruitment contribute to myocardial macrophage expansion in chronic heart failure. Circ Res 2016;119:853–864.
21. van den Akker F, Deddens JC, Doevendans PA, et al. Cardiac stem cell therapy to modulate inflammation upon myocardial infarction. Biochim Biophys Acta 2013;1830:2449–2458.
22. Hamid T, Prabhu SD. Immunomodulation is the key to cardiac repair. Circ Res 2017;120:1530–1532.
23. Lopez JJ, Laham RJ, Stamler A, et al. VEGF administration in chronic myocardial ischemia in pigs. Cardiovasc Res 1998;40:272–281.
24. Henry TD, Annex BH, McKendall GR, et al. The VIVA trial: vascular endothelial growth factor in ischemia for vascular angiogenesis. Circulation 2003;107:1359–1365.
25. Zangi L, Lui KO, von Gise A, et al. Modified mRNA directs the fate of heart progenitor cells and induces vascular regeneration after myocardial infarction. Nat Biotechnol 2013;31:898–907.
26. Pacak CA, Mah CS, Thattaliyath BD, et al. Recombinant adeno-associated virus serotype 9 leads to preferential cardiac transduction *in vivo*. Circ Res 2006;99:e3–9.
27. Vassalli G, Bueler H, Dudler J, et al. Adeno-associated virus (AAV) vectors achieve prolonged transgene expression in mouse myocardium and arteries *in vivo*: a comparative study with adenovirus vectors. Int J Cardiol 2003;90:229–238.
28. Kocher AA, Schuster MD, Szabolcs MJ, et al. Neovascularization of ischemic myocardium by human bone-marrow-derived angioblasts prevents cardiomyocyte apoptosis, reduces remodeling and improves cardiac function. Nat Med 2001;7:430–436.
29. Bartunek J, Vanderheyden M, Vandekerckhove B, et al. Intracoronary injection of CD133-positive enriched bone marrow progenitor cells promotes cardiac recovery after recent myocardial infarction: feasibility and safety. Circulation 2005;112: I178–183.
30. Takahashi M, Li TS, Suzuki R, et al. Cytokines produced by bone marrow cells can contribute to functional improvement of the infarcted heart by protecting cardiomyocytes from ischemic injury. Am J Physiol Heart Circ Physiol 2006;291:H886–893.
31. Tengood JE, Kovach KM, Vescovi PE, et al. Sequential delivery of vascular endothelial growth factor and sphingosine 1-phosphate for angiogenesis. Biomaterials 2010;31:7805–7812.
32. Gkontra P, Norton KA, Zak MM, et al. Deciphering microvascular changes after myocardial infarction through 3D fully automated image analysis. Sci Rep 2018;8:1854.
33. Squadrito ML, Pucci F, Magri L, et al. miR-511-3p modulates genetic programs of tumor-associated macrophages. Cell Rep 2012;1:141–154.
34. Baker M, Robinson SD, Lechertier T, et al. Use of the mouse aortic ring assay to study angiogenesis. Nat Protoc 2011;7:89–104.
35. Schindelin J, Arganda-Carreras I, Frise E, et al. Fiji: an open-source platform for biological-image analysis. Nat Methods 2012;9:676–682.
36. Prabhu SD, Frangogiannis NG. The biological basis for cardiac repair after myocardial infarction: from inflammation to fibrosis. Circ Res 2016;119: 91–112.

37. Talman V, Ruskoaho H. Cardiac fibrosis in myocardial infarction—from repair and remodeling to regeneration. Cell Tissue Res 2016;365:563–581.

38. Fan H, Ma L, Fan B, et al. Role of PDGFR-beta/PI3K/AKT signaling pathway in PDGF-BB induced myocardial fibrosis in rats. Am J Transl Res 2014; 6:714–723.

39. Mostaco-Guidolin L, Rosin NL, Hackett TL. Imaging collagen in scar tissue: developments in second harmonic generation microscopy for biomedical applications. Int J Mol Sci 2017;18.

40. Azevedo PS, Polegato BF, Minicucci MF, et al. Cardiac remodeling: concepts, clinical impact, pathophysiological mechanisms and pharmacologic treatment. Arq Bras Cardiol 2016;106: 62–69.

41. De Celle T, Cleutjens JP, Blankesteijn WM, et al. Long-term structural and functional consequences of cardiac ischaemia–reperfusion injury *in vivo* in mice. Exp Physiol 2004;89:605–615.

42. Silvestre JS, Smadja DM, Levy BI. Postischemic revascularization: from cellular and molecular mechanisms to clinical applications. Physiol Rev 2013;93:1743–1802.

43. Dube KN, Thomas TM, Munshaw S, et al. Recapitulation of developmental mechanisms to revascularize the ischemic heart. JCI Insight 2017;2.

44. Schuleri KH, Amado LC, Boyle AJ, et al. Early improvement in cardiac tissue perfusion due to mesenchymal stem cells. Am J Physiol Heart Circ Physiol 2008;294:H2002–2011.

45. Zakrzewicz A, Secomb TW, Pries AR. Angioadaptation: keeping the vascular system in shape. News Physiol Sci 2002;17:197–201.

46. Hao X, Mansson-Broberg A, Gustafsson T, et al. Angiogenic effects of dual gene transfer of bFGF and PDGF-BB after myocardial infarction. Biochem Biophys Res Commun 2004;315:1058–1063.

47. Banquet S, Gomez E, Nicol L, et al. Arteriogenic therapy by intramyocardial sustained delivery of a novel growth factor combination prevents chronic heart failure. Circulation 2011;124:1059–1069.

48. Forte E, Furtado MB, Rosenthal N. The interstitium in cardiac repair: role of the immune-stromal cell interplay. Nat Rev Cardiol 2018;15:601–616.

49. Baluk P, Lee CG, Link H, et al. Regulated angiogenesis and vascular regression in mice overexpressing vascular endothelial growth factor in airways. Am J Pathol 2004;165:1071–1085.

50. Sano H, Hosokawa K, Kidoya H, et al. Negative regulation of VEGF-induced vascular leakage by blockade of angiotensin II type 1 receptor. Arterioscler Thromb Vasc Biol 2006;26:2673–2680.

51. Waeber C, Walther T. Sphingosine-1-phosphate as a potential target for the treatment of myocardial infarction. Circ J 2014;78:795–802.

52. Jung K, Kim P, Leuschner F, et al. Endoscopic time-lapse imaging of immune cells in infarcted mouse hearts. Circ Res 2013;112:891–899.

53. Park Y, Lee J, Kwak JY, et al. Fractalkine induces angiogenic potential in CX3CR1-expressing monocytes. J Leukoc Biol 2018;103:53–66.

54. Getzin T, Krishnasamy K, Gamrekelashvili J, et al. The chemokine receptor CX3CR1 coordinates monocyte recruitment and endothelial regeneration after arterial injury. EMBO Mol Med 2018;10: 151–159.

55. Hughes JE, Srinivasan S, Lynch KR, et al. Sphingosine-1-phosphate induces an antiinflammatory phenotype in macrophages. Circ Res 2008;102:950–958.

56. Sager HB, Hulsmans M, Lavine KJ, et al. Proliferation and recruitment contribute to myocardial macrophage expansion in chronic heart failure. Circ Res 2016;119:853–864.

57. Wong SP, French JK, Lydon AM, et al. Relation of left ventricular sphericity to 10-year survival after acute myocardial infarction. Am J Cardiol 2004; 94:1270–1275.

58. van den Borne SW, Diez J, Blankesteijn WM, et al. Myocardial remodeling after infarction: the role of myofibroblasts. Nat Rev Cardiol 2010;7:30–37.

59. Aguero J, Lobo Gonzalez M, Ishikawa K. Route TESI: main street for MSC? Circ Res 2017;120: 1055–1056.

60. Meyer GP, Wollert KC, Lotz J, et al. Intracoronary bone marrow cell transfer after myocardial infarction: 5-year follow-up from the randomized-controlled BOOST trial. Eur Heart J 2009;30: 2978–2984.

61. Assmus B, Rolf A, Erbs S, et al. Clinical outcome 2 years after intracoronary administration of bone marrow-derived progenitor cells in acute myocardial infarction. Circ Heart Fail 2010;3:89–96.

62. Wollert KC, Meyer GP, Lotz J, et al. Intracoronary autologous bone-marrow cell transfer after myocardial infarction: the BOOST randomised controlled clinical trial. Lancet 2004;364:141–148.

63. Schachinger V, Erbs S, Elsasser A, et al. Intracoronary bone marrow-derived progenitor cells in acute myocardial infarction. N Engl J Med 2006;355:1210–1221.

Received for publication September 21, 2018;
accepted after revision February 12, 2019.

Published online: February 15, 2019.